Turkish Journal of Engineering & Environmental Sciences

http://journals.tubitak.gov.tr/engineering/

Research Article

Turkish J Eng Env Sci
(2014) 38: 79 – 96

doi:10.3906/muh-1402-13

Thermal modeling during continuous ultrasonic welding

Ömer Sinan ŞAHİN[1,*], Steve KOELLHOFFER[2], John GILLESPIE[2], Suresh ADVANI[2], Travis BOGETTI[3]

[1]Mechanical Engineering Department, Engineering Faculty, Selçuk University, Konya, Turkey
[2]Center for Composite Materials, University of Delaware, Newark, Delaware, USA
[3]Army Research Laboratory, Aberdeen Proving Ground, Aberdeen, Maryland, USA

Received: 25.02.2014 • **Accepted:** 23.07.2014 • **Published Online:** 24.10.2014 • **Printed:** 21.11.2014

Abstract: In this study, a thermal model during continuous ultrasonic welding of thin foils has been developed. The heat generation during the process, stick/slip state, and effect of elastic/plastic strains are included in the formulation. The physics is simplified to a one-dimensional transient heat transfer analysis, the governing equation is nondimensionalized, and important parameters are identified. A fourth-order Runge–Kutta numerical scheme is used to predict the transient temperature as a function of material, constitutive, and process parameters. Comparison with experimental results is provided to justify the assumptions introduced in the model. Different heat generation terms are introduced and their contribution to overall heat generation is presented.

Key words: Ultrasonic welding, thermal model, heat generation, computation

1. Introduction

Ultrasonic consolidation is a relatively new technique that can be used to bond both similar and dissimilar materials that may otherwise be difficult to weld by conventional welding and casting techniques. The process temperature is not as high as in other welding techniques, and thus the process reduces residual thermal stresses in the proximity of the welded region.

The ultrasonic consolidation process is schematically shown in Figure 1. The experimental apparatus consists of a substrate material that is mounted on an anvil, a metal foil or a metal foil reinforced with continuous fibers to be welded, and a sonotrode attached to the ultrasonic bonding unit. The materials to be bonded are introduced between the sonotrode and the stationary anvil. As depicted, the consolidation is induced by a sonotrode that oscillates at a high frequency in the direction perpendicular to rolling. The sonotrode also applies a load on the material in the vertical direction, which creates a normal force and induces oscillating shear forces due to interface friction between the surfaces to be bonded. The materials to be welded also plastically deform under this oscillatory action. The interfacial shear forces and the yielding phenomenon break up surface oxides and contaminants. The elastic and thermal mismatches between the oxides and the base metal help this removal process [1]. This surface cleanup process is essential for atomic bonding, which generally depends on close contact and a surface area free of oxides and contaminants available for atomic diffusion [2]. It is reported that no surface preparation prior to consolidation is necessary [3] even if a tenacious oxide layer is present. However, surface preparation is recommended since it has been reported to improve the bonded area by approximately 45% [1].

*Correspondence: ossahin@selcuk.edu.tr

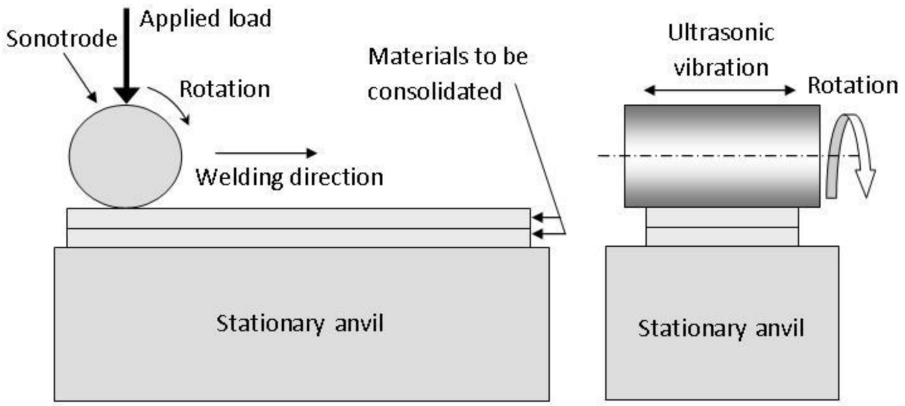

Figure 1. Schematic representation of welding.

The ultrasonic bonding mechanism is reported to be a repetitive stick-slip [4] mechanism. The surface asperities bond together by means of friction during the stick phase and create contact points. The contact points shear and break during the slip phase [5]. In the slip phase, the surface deformation increases and the oxide film on the mating surfaces breaks and displaces. As the process repeats, the contact points increase in both number and cross-sectional area. Continuous formation and breakage of contact points results in strain hardening, which leads to an increase in the weld strength.

Vairis et al. [6] established analytical and numerical models for linear friction welding of Ti6Al4V to predict process temperatures. Midling et al. developed a process model to predict microstructure and strength [7]. Others have investigated the temperature distribution [8] during friction welding of AI-Mg-Si alloys and AI-SiC metal matrix composites. Cheng [9] et al. explored the amount of heat generation using microsensor analysis in ultrasonic metal welding.

The ultrasonic welding (UW) process has been successfully used for consolidation of polymeric materials [10,11]. It was reported [7] that this is also an ideal joining process for aluminum alloys and aluminum matrix composites since the materials to be consolidated do not have to be heated to their melt temperature. It is as effective as friction welding, especially for aluminum and its alloys.

Elangovan et al. [12] and Sriraman et al. [13] studied the temperature distribution during ultrasonic welding. Siddiq et al. [14] investigated UW by considering the acoustic softening effect.

Even though the UW process has been used in industry, the basic mechanisms that define the process physics are not fully understood [15]. Although there have been attempts in the literature to obtain a comprehensive process model for UW, there remain ambiguities that need to be clarified, such as heat generation characteristics and weld area development. The repetitive stick-slip [4] mechanism is one way to explain the ultrasonic bonding phenomenon. As the process continues, the temperature of the material increases and reduces the energy required for further deformation and breaking of the microbonds. The heat generated during ultrasonic consolidation is also important and has been studied [16,17].

In this study, the heat generation and temperature increase characteristics during the UW process have been investigated. The heat generation term has been formulated as a sum of deformational heat generation and frictional heat generation. The elastic strain energy that is converted into heat is also formulated and found to be insignificant under certain conditions. The overall heat generation model accounts for the stick/slip phase changes. The governing temperature equation was solved in nondimensional form using the fourth-order Runge–Kutta method and the results are presented and discussed.

2. Parameters

A schematic representation of the continuous ultrasonic welder is shown in Figure 1. As seen in this figure, the materials to be welded are kept stationary by the anvil and the sonotrode applies vibration across the width of the sample transverse to the welding direction while simultaneously applying a vertical load while rolling. Parameters affecting the weld quality can be divided into 2 groups: "material and geometric parameters" and "process parameters". These parameters are shown in Table 1.

Table 1. Material and process variables.

• Material and geometric variables • Material • Part dimensions • Surface quality • Hardness • Surface oxides	• Process variables • Clamping methodology • Applied load • Horn type • Vibration amplitude • Vibration frequency • Process duration • Energy directors

3. Heat generation

The temperature of the metals in contact is increased due to both friction and deformation. The plastic deformation can be included in the model as a volumetric heat generation term, whereas friction at the interface between 2 surfaces being bonded is addressed as heat flux supplied at the interface. In this section, the heat flux and generation terms are formulated. The applied vibration produces 3 different deformations: slip between mating surfaces, elastic shear deformation, and plastic shear deformation. The applied amplitude is the sum of 3 separate displacements: $\delta_{app} = \delta_{slip} + \delta_{elastic\,shear} + \delta_{plastic\,shear}$. The following sections define the heat generation terms and divide the applied vibration amplitude into its subcomponents and use it to estimate the individual contribution of these deformations to heat generation.

3.1. Frictional heat flux

The applied vibration amplitude consists of 2 parts, a slip component and a shear component. However, for the sake of simplicity the shear component is ignored and applied vibration amplitude is considered to create slip motion between mating surfaces. The rate of energy or power generated at the interface due to the rubbing of the 2 mating surfaces as induced by the sonotrode can be regarded as the product of the friction force and the average horn speed:

$$P = F_{FR}.v_{avg}. \tag{1}$$

The average horn speed can be calculated by using the following formula [15]:

$$v_{avg} = 4.\delta_{Slip}.f, \tag{2}$$

where δ_{Slip} is the slip distance and f is the frequency of the sonotrode. The frictional power input can be considered as a heat flux over the deformation zone, which is expressed as:

$$\dot{q}_{FR} = \frac{P}{A_{DZ}}. \tag{3}$$

Combining previous equations and rewriting the heat flux in terms of process and material parameters, we get:

$$\dot{q}_{FR} = \frac{4.\delta_{Slip}.f.F_{ap}.\mu}{A_{Dz}}. \tag{4}$$

Here F_{FR} in Eq. (1) is replaced with friction coefficient μ times the applied normal force F_{ap}. The friction coefficient greatly affects the shear force between mating surfaces and may change during the UW process. For the sake of simplicity, the friction coefficient is assumed to be constant. q_{FR} is applied as the heat flux boundary condition at the interface of the 2 foils when predicting the temperature field.

3.2. Volumetric heat generation due to deformation

The deformation zone that undergoes plastic deformation [15] is assumed to contribute to energy transfer by converting the deformational energy into volumetric heat generation.

3.2.1. Heat generation due to plastic deformation

The differential shear element under compression shown in Figure 2 can be used to calculate the heat generated due to plastic deformation. Due to symmetry, the formulation is developed for a single foil of thickness L.

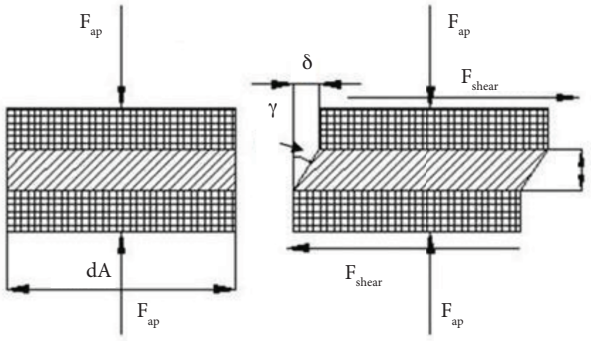

Figure 2. Differential element under shear deformation.

By assuming elastic-perfectly plastic behavior, the work done within this shear element can be expressed as:

$$\frac{dW}{dV} = \tau_y * \gamma. \tag{5}$$

Now we can derive Eq. (5) with respect to time [15] and get the power input for differential volume. We can also express the shear angle (γ) in terms of deformation by plastic shear and foil thickness as:

$$\frac{\Delta dW}{dt} * \frac{1}{dV} = \tau_y * \frac{\Delta\delta_{Shear\_p}}{\Delta t * L}. \tag{6}$$

Thus, the dissipated volumetric energy over time (power) over the volume of differential shear element is written as:

$$\dot{q}_w = \frac{dP}{dV} = \tau_y * \frac{v_{avg}}{L}. \tag{7}$$

The average speed can also be expressed in terms of the frequency as presented in [15]:

$$v_{avg} = 4.\delta_{Shear\_p}.f.$$

Since shear strength of the material (τ_y) is temperature-dependent, the heat generation by plastic deformation (q_w) will also be temperature-dependent. Figure 3 is an interpretation of Eq. (7) and shows the variation of this term versus temperature for different amplitude/foil thickness values. This figure shows the potential contribution of q_w to overall heat generation. At higher temperatures, q_w decreases dramatically due to the decrease of shear strength of material with temperature.

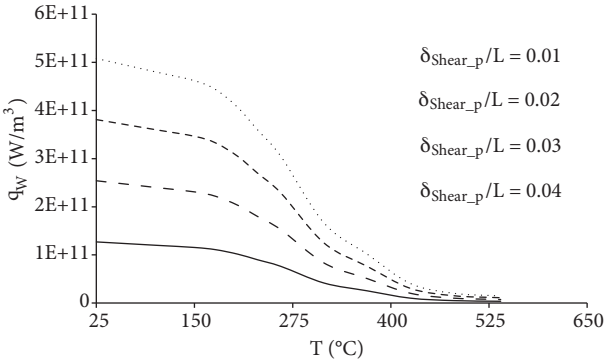

Figure 3. Variation in volumetric heat generation due to plastic deformation as a function of temperature (foil thickness: 100 μmsgf = 20,000 Hz, yield strength at room temperature = 158 MPa, material: aluminum 6061-T6).

Some researchers have incorporated this deformational heat input as a surface heat flux [15]. For the case of the deformational heat generation being modeled as surface heat flux, the weld area needs to be clearly identified and is independent of the thickness of the foil. We model the deformational heat input as a volumetric phenomenon, thus allowing us to include the effect of thickness, which is known to influence the temperature field and the weld quality.

3.2.2. Heat generation due to elastic hysteresis

The applied vibration amplitude can lead to elastic strain or plastic strain depending on the foil thickness. The elastic strain energy is recovered but the elastic strain can cause elastic hysteresis, which is dissipated as heat. The generated heat generally manifests itself as thermoelastic effect [18]. The dissipated energy within the material can be calculated as the product of applied strain energy times specific damping ratio (ψ), which represents the amount of heat dissipated due to internal friction in each cycle. Strain energy for the differential element shown in Figure 2 can be written as:

$$U = \frac{F_{shear}}{2}.\delta_{Shear\_e} = \frac{\mu.F_{ap}}{2}.\delta_{Shear\_e}. \tag{8}$$

Thus, the generated power will be:

$$P = \frac{dU}{dt} = \frac{\mu.F_{ap}}{2}.\frac{d\delta_{Shear\_e}}{dt} \tag{9}$$

as

$$\frac{d\delta}{dt} = v_{avg} = 4.\delta_{Shear\_e}.f. \tag{10}$$

One can insert Eq. (10) into Eq. (9) to obtain the heat generated due to the shear stress when in the elastic range:

$$P = \frac{\mu.F_{ap}}{2}.4.\delta_{Shear\_e}.f = 2.\mu.F_{ap}.\delta_{Shear\_e}.f. \tag{11}$$

The dissipated energy will be the product of the power in Eq. (11) and the specific damping ratio (ψ), which will be dissipated over the volume of differential shear element. So, the volumetric heat generation rate is:

$$\dot{q}_{eh} = \psi.\frac{P}{V} = \psi.\frac{2.\mu.F_{ap}.\delta_{Shear\_e}.f}{L.A_{Dz}} = \psi.\frac{2.\mu.F_{ap}.f}{A_{Dz}}.\frac{\delta_{Shear\_e}}{L}. \tag{12}$$

Since $G = \frac{\tau}{\gamma} = \frac{\mu.F_{ap}/A_{DZ}}{\delta_{Shear\_e}/L}$, therefore $\frac{\delta_{Shear\_e}}{L} = \frac{\mu.F_{ap}/A_{DZ}}{G}$, and one can then recast the expression for volumetric heat generation due to elastic hysteresis as follows:

$$\dot{q}_{eh} = \psi.\frac{2.\mu.F_{ap}.f}{A_{Dz}}.\frac{\mu.F_{ap}/A_{DZ}}{G} = \psi.\frac{2.\mu^2.F_{ap}^2.f}{A_{DZ}^2.G}. \tag{13}$$

The shear modulus (G) is also a function of temperature, so the heat generation term due to damping within the elastic limit can be written as:

$$\dot{q}_{eh} = \psi.\frac{2.\mu^2.F_{ap}^2.f}{A_{DZ}^2.G(T)}. \tag{14}$$

The elastic limit for vibration amplitude can be written as:

$$\frac{\delta_{\max}}{L} = \gamma = \frac{\tau_y(T)}{G(T)}. \tag{15}$$

Hence, for the material to exhibit elastic deformation, $\frac{\delta_{app}}{L} \leq \frac{\tau_{ap}(T)}{G(T)}$ must be satisfied. A new function is defined to show temperature-dependent property changes:

$$K(T) = \frac{\tau_{ap}(T)}{G(T)}. \tag{16}$$

This function is used in a later section where nondimensional analysis is introduced. Figure 4 is obtained by evaluation of Eq. (15) and shows the elastic strain limits for different foil thicknesses at different temperatures. As seen from this figure, the maximum allowable amplitude value increases as the part thickness increases. However, the maximum allowable amplitude decreases as the temperature of the material increases and materials soften. For a given part thickness, the material undergoes plastic deformation for even relatively small vibration amplitudes. Given that most UW is done above 6 μm and with materials smaller than 1 mm in thickness, one can conclude that elastic properties of materials to be welded are not of great importance in dissipation of heat during the welding process.

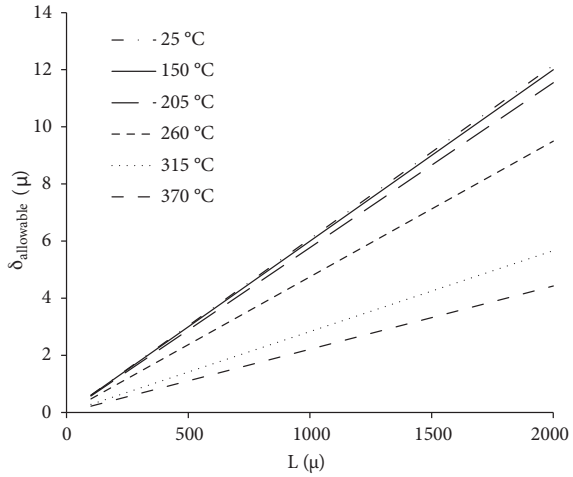

Figure 4. Maximum allowable vibration amplitude for elastic deformation (aluminum 6061-T6).

4. Determination of slip/stick state

The repetitive stick/slip mechanism at the interface is the best way to explain the bonding mechanism of ultrasonic consolidation [4]. The applied normal force of the sonotrode as shown in Figure 5 generates a frictional shear stress at the interface of materials to be welded. It is determined by this shear stress whether slip or stick phase will take place at the interface.

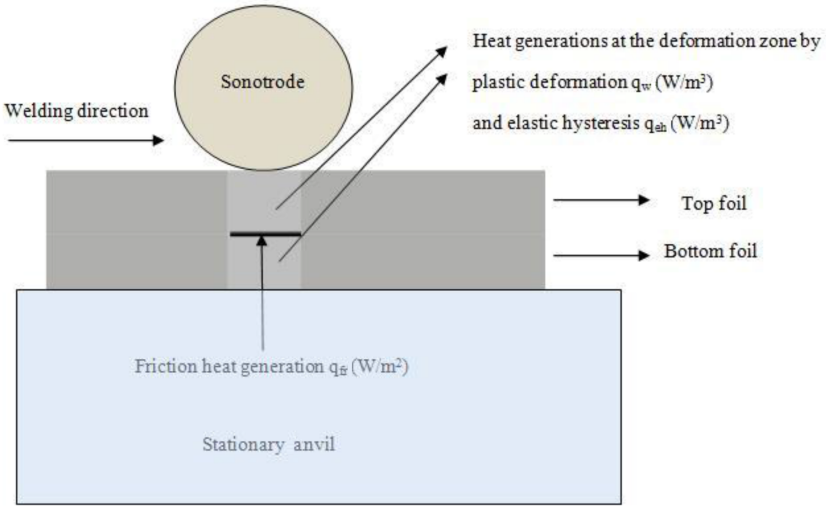

Figure 5. Schematic of heat inputs and parts considered for parametric study (not drawn to scale).

The slip/stick state must be determined and continuously controlled during calculation since different amounts of heat are generated at stick and slip phases.

Maalekian et al. [19] defined a state variable that determines whether slip or stick will take place. Figure 6 represents the definition of a Dirac delta function that defines the change from slip to stick for aluminum 6061-T6. Full sticking occurs when $\Delta = 1$ and full slip occurs when $\Delta = 0$. Maalekian et al. [19] also showed that there should be a transition region from the full slip to full stick state. However, this transition behavior has been ignored for the sake of simplicity.

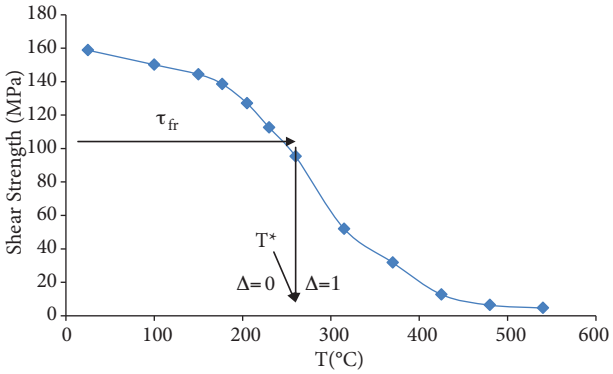

Figure 6. Shear stress value when the slipping between the surfaces changes to sticking as a function of temperature. Material: aluminum 6061-T6 (reference data from Maalekian et al. [15]).

By the graphical definition, for a given applied load, the slip state changes into stick state at a critical temperature (T*). It can be concluded that slip occurs when $T < T^*$ and sticking takes place when $T \geq T^*$. The critical temperature for stick (T*) can be easily found since the shear strength versus temperature of aluminum alloy is known (Figure 6). For numerical calculations, temperature-dependent shear strength of aluminum alloy was expressed in terms of nondimensional temperature by means of curve-fitting.

The stick phase is a prerequisite for bond formation, so the interface temperature must be greater than the critical temperature for bonding. On the other hand, heat generation terms also depend on slip/stick state, as described in Figure 7. In this study, slip/stick state has been obtained by the method proposed by Maalekian et al. [19]. The slip/stick state and heat generation have been updated at each step of calculation as shown in Figures 7 and 8. The resulting overall heat generation in terms of slip/stick state is summarized in Eq. (17).

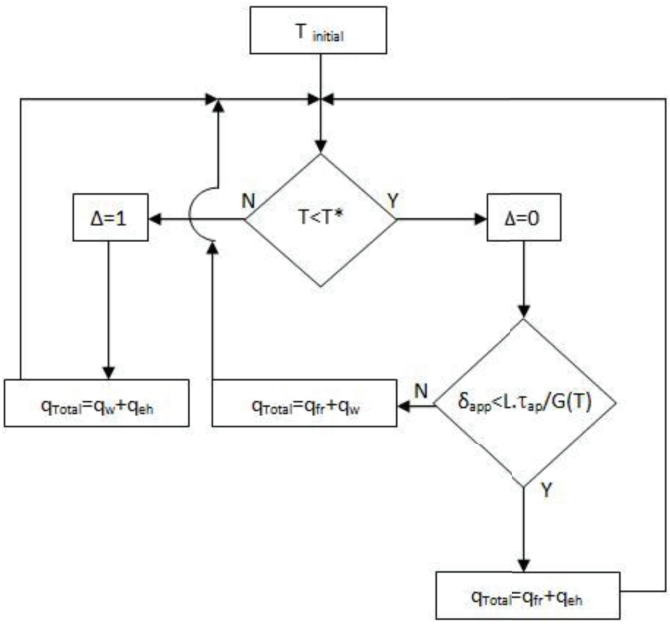

Figure 7. Flow chart that addresses the heat generation during UW process as a function of temperature.

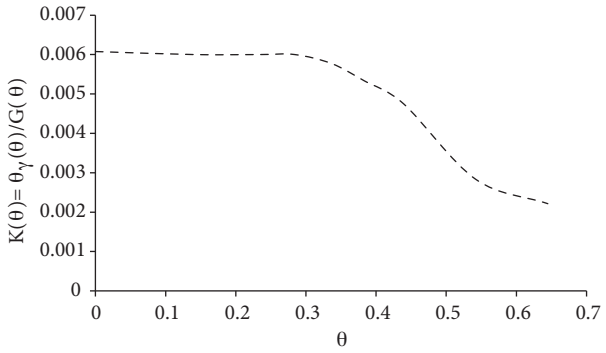

Figure 8. K (θ) versus nondimensional temperature (θ) for aluminum 6061-T6.

The assumptions of the analysis are as follows:

- There is no slip between sonotrode and top surface of the top foil.
- Initially there is friction between foils to be welded until they stick.

By using these assumptions, the overall heat generation equation during UW was derived as described here.

5. Summary of heat generation terms

There are 3 different kinds of heat generation in the UW process. They are:

- Frictional heat generation (q_{FR}) (heat flux at the interface).
- Heat generation by plastic deformation (q_W) (volumetric heat generation at the deformed volume).
- Heat generation by elastic hysteresis (q_{eh}) (volumetric heat generation at the deformed volume, typically negligible).

The total heat generation is a combination of these heat generations depending on the state variable (Δ). At the initial stage of welding, only the slip state occurs ($\Delta = 0$). Since the foils are not yet sticking, heat is generated due to friction (q_{FR}). In this stage, if applied vibration amplitude is within elastic limits of the material, additional heat generation by elastic hysteresis (q_{eh}) can arise, or else the material will deform plastically, which results in heat generation by plastic deformation (q_W). The criterion for determining this situation is to check whether $\delta_{app} < L\tau_{ap}$/G(T).

The heat generation results in temperature increase and determines whether the interface temperature will increase above T* and invoke the stick phase ($\Delta = 1$). Once T > T*, the state variable Δ will be equal to 1, which means the 2 foils are stuck together and additional heat enters the system only through heat generation due to plastic deformation (q_W) and heat generation due to elastic hysteresis (q_{eh}). Figure 7 summarizes the heat generation during the UW process. As discussed in Section 3.2.2, heat generation by elastic hysteresis (q_{eh}) has a negligible effect. Therefore, this heat generation term is disregarded in the developed numerical solution.

Total heat generation can be expressed as follows:

$$q = \left\{ \begin{array}{l} \Delta = 0 \rightarrow q = (\frac{\mu.F_{ap}.4.\delta_{Slip}.f}{A_{Dz}})_S + \left(\begin{array}{l} \delta_{app} \leq \frac{L.\tau_{ap}}{G(T)} \Rightarrow (\frac{2.\mu^2.F_{ap}^2.f}{A_{DZ}^2.G(T)})_V \\ \delta_{app} > \frac{L.\tau_{ap}}{G(T)} \Rightarrow (\frac{\tau_y(T).4.\delta_{Shear\_p}.f}{L})_V \end{array} \right) \quad (17a) \\ \Delta = 1 \rightarrow \Rightarrow q = (\frac{\tau_y(T).4.\delta_{Shear\_p}.f}{L})_V \quad (17b) \end{array} \right\}.$$

The second term on the right-hand side in Eq. (17a), q_{eh}, is ignored as we have determined that it makes very little contribution to the heat input to the system. In order for foils to deform plastically, either the applied shear stress must exceed the elastic limits of the material or the foils have to be at a temperature higher than T*. By noting that, applied vibration amplitude creates 3 different deformations, which can be quantified as follows:

$$\delta = \left\{ \begin{array}{l} \Delta = 0 \rightarrow \left(\begin{array}{l} \delta_{app} < \frac{L.\tau_{ap}}{G(T)} \Rightarrow \delta_{app} = \delta_{slip} + \delta_{shear\_e} \\ \delta_{app} \geq \frac{L.\tau_{ap}}{G(T)} \Rightarrow \delta_{app} = \delta_{slip} + \delta_{shear\_e} + + \delta_{shear\_p} \end{array} \right) \quad (18a) \\ \Delta = 1 \rightarrow \delta_{app} = \delta_{shear\_e} + \delta_{shear\_p} \quad (18b) \end{array} \right\}.$$

As stated in Section 3, the applied amplitude is distributed between various subcomponents that need to be determined. These subcomponents are used to evaluate different heat generation terms that arise during UW. Since the temperature-dependent material properties are known, δ_{shear_e} can be calculated. It is assumed that δ_{Slip} and δ_{Shear_p} are equal when $\Delta = 0$ and $\delta_{app} \geq \frac{L.\tau_{ap}}{G(T)}$.

6. Parametric study

In the preceding section, the heat generated during UW was expressed in terms of the ultrasonic consolidation machine process variables and material properties. The solution of the energy equation with the heat input expressed in Eq. (17) is a time- and material-dependent problem. To obtain a general solution we will nondimensionalize the equation. To derive the energy balance it is assumed that temperature does not change with position. This assumption is valid due to the small sample dimensions and high amounts of internal heat conduction present during UW that result in a low Biot number, which justifies the use of the lumped parameter analysis. The resulting energy balance of a differential element as shown in Figure 2 can be expressed as follows:

$$q_f + q_w L = h(T - T\infty) + \rho L C_p \frac{dT}{dt}. \quad (19)$$

Here h represents a convective loss term that accounts for losses to air and contacting surfaces. This term depends on contact area and geometry of adjacent materials and their thermal conductivity, and it will be time-dependent as the temperature of the other bodies in contact does change with time.

To nondimensionalize the dependent and independent variables t and T, the following is proposed:

$$t^{\wedge} = \frac{t}{t_c} \text{ and } \theta = \frac{T - T_\infty}{T_m - T_\infty}.$$

The energy balance can then be expressed as:

$$q_f + q_w.L = h.\theta.(T_m - T_\infty) + \rho.C_P L.(T_m - T_\infty).\frac{d\theta}{dt}. \quad (20)$$

By making algebraic modifications, the following equation can easily be obtained in nondimensional form:

$$\frac{q_f + q_w.L}{h(T_m - T_\infty)} = \theta + \frac{\rho.C_P L}{ht_c}\frac{d\theta}{dt^\wedge}. \tag{21}$$

As shown in Eq. (14), the heat generation through elastic deformation is temperature-dependent. Numerical calculations showed that the contribution of this heat generation term is less than 5% for the input parameters used in simulation. It is thus concluded that it can be neglected. Now we can rearrange the overall heat generation in terms of frictional and volumetric heat generation terms, which yields:

$$q = \left\{ \begin{array}{l} \Delta = 0 \rightarrow \left\{ \begin{array}{l} \delta_{app} \leq \frac{L.\tau_{ap}}{G(T)} \rightarrow q = \dot{q}_{fr} \\ \delta_{app} > \frac{L.\tau_{ap}}{G(T)} \rightarrow q = \dot{q}_{fr} + \dot{q}_w \end{array} \right\} \\ \Delta = 1 \rightarrow \{q = \dot{q}_w\} \end{array} \right\}. \tag{22}$$

Referring to Figure 7, it is seen that as the mechanism changes from slip to stick, the heat input terms need to be updated. Thus, the equation that needs to be solved is written in nondimensional form as:

$$\left\{ \begin{array}{l} \theta < \theta^* \rightarrow \left\{ \begin{array}{l} \delta_{app} \leq \frac{L.\tau_{ap}}{G(\theta)} \rightarrow \frac{q_f}{h(T_m - T_\infty)} = \theta + \frac{\rho C_p L}{h.t_c}\frac{d\theta}{dt^\wedge} \\ \delta_{app} > \frac{L.\tau_{ap}}{G(\theta)} \rightarrow \frac{q_f + q_w(\theta)L}{h(T_m - T_\infty)} = \theta + \frac{\rho C_p L}{h.t_c}\frac{d\theta}{dt^\wedge} \end{array} \right\} \\ \theta \geq \theta^* \rightarrow \frac{q_w(\theta)L}{h(T_m - T_\infty)} = \theta + \frac{\rho C_p L}{h.t_c}\frac{d\theta}{dt^\wedge} \end{array} \right\}. \tag{23}$$

Here θ^* represents the critical point for slip/stick phase change in terms of nondimensional temperature.

The variation of K(θ) for aluminum 6061-T6 was calculated by evaluating the temperature-dependent properties of the material and is shown in Figure 8. In order to use K(θ) for numerical solutions in conjunction with the flow chart in Figure 7, the Harris model ($K(\theta) = \frac{1}{(a+b\theta^c)}$) was used to fit the experimental data and determine the coefficients (a = 0.00630, b = 0.15742, and c = 4.20510). The fitted equation is shown in Figure 8.

From Eq. (23), we can define 2 new nondimensional parameters:

$$P_1 = \frac{q_f + q_w.L}{h(T_m - T_\infty)}, \tag{24}$$

$$P_2 = \frac{\rho.C_P L}{ht_c}, \tag{25}$$

where Tm and T∞ are the material's melting temperature and ambient temperature, respectively. P_1 represents the ratio of the overall heat generation, which includes both frictional heat generation at the interface and volumetric heat generation due to plastic shear deformation and the dissipated heat to the surroundings. Therefore, P_1 determines if the system is transient ($P_1 > 1$) or steady-state ($P_1 = 1$). This can also be considered as a "heat accumulation coefficient". P_2 represents the contribution of the time-dependent term, which will vanish as the system approaches the steady state. The characteristic time can be chosen such that P_2 is always equal to 1. This allows us to choose the characteristic time, t_c, as:

$$t_c = \frac{\rho.C_P L}{h}. \tag{26}$$

One can now conduct the nondimensional analysis as a function of P_1, which states how heat generated gets dissipated. Note in this analysis that the heat transfer coefficient h is assumed to be a constant, which may not be a very good assumption but does allow us to examine the system in an approximate fashion.

For solving these equations, the fourth-order Runge–Kutta method was used. The flow chart for this analysis is shown in Figure 9. As seen in this figure, the user enters the process parameters. If the applied vibration amplitude does not exceed the elastic limits of the material, the left branch of the flow chart will be executed. If the material deforms only elastically, there is only frictional heat generation. If the applied vibration amplitude exceeds the elastic limits of the material, the right branch of flow chart will be executed. This means that there are both frictional heat generation and deformational heat generation. Thus, both of them must be included in overall heat generation.

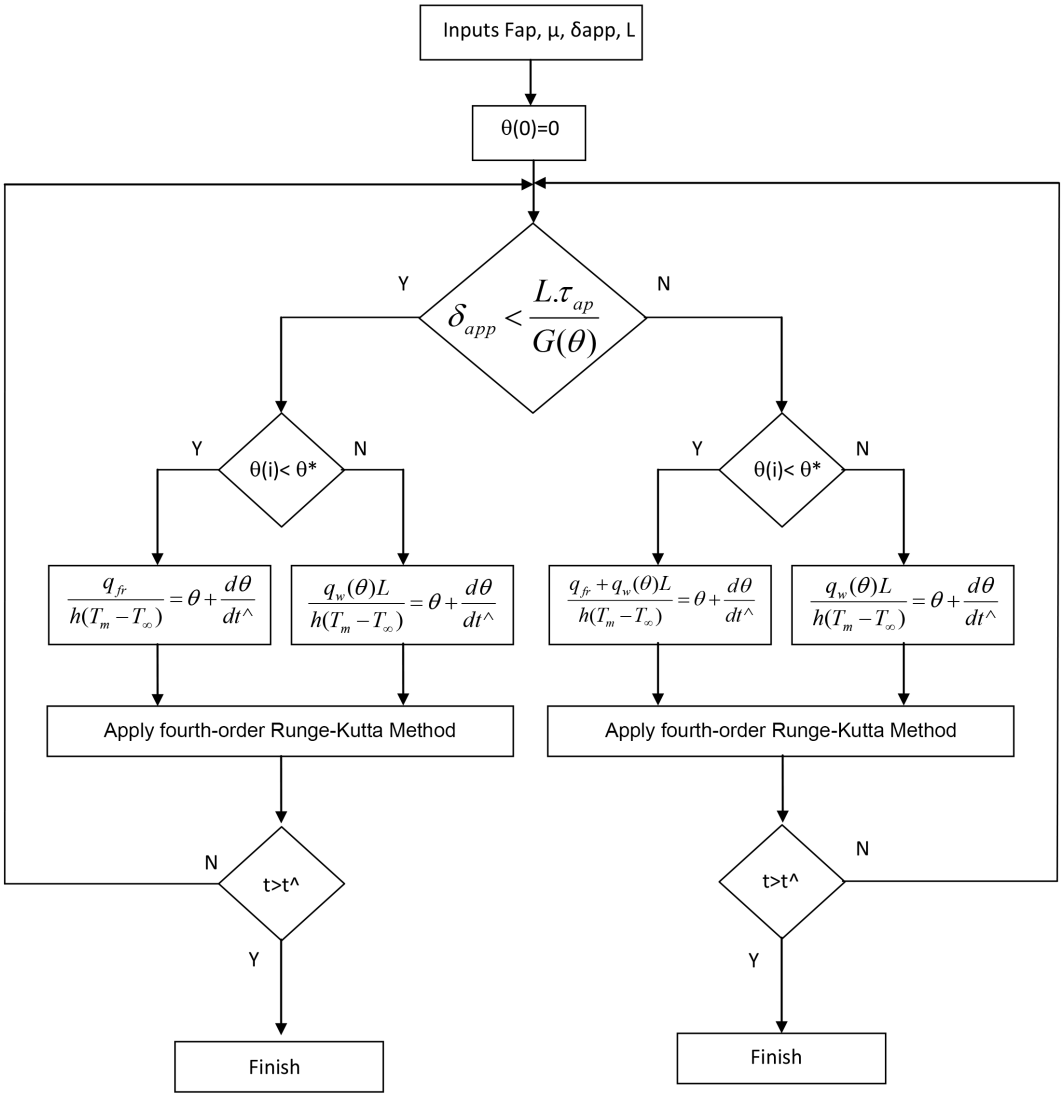

Figure 9. Numerical solution flowchart.

The condition of $\theta < \theta^*$ determines whether $\Delta = 0$ or $\Delta = 1$ (see Figure 6). If $\Delta = 0$ the foils are not sticking and there is friction between them. If $\theta \geq \theta^*$ ($\Delta = 1$), the foils are stuck together and there is no heat

generation due to friction as there is no relative motion between the 2 foils. At each time step, the algorithm determines whether $\theta < \theta^*$ by using the variation of the material's yield strength versus the temperature graph given in Figure 6.

Eq. (23) is nondimensional. However, the terms q_w and q_f in Eq. (23) depend upon applied force and sonotrode velocity. Since the power input to the system is a product of applied force times sonotrode velocity, a nondimensional parameter that includes both applied force and sonotrode velocity can be used to define the power input. By introducing the parameter $(P^{\wedge})$, variations in the applied force and sonotrode velocity can be quantified using this nondimensional parameter for power input.

$$P^{\wedge} = \frac{F_{ap}.V_{avg}}{A_{DZ}.h(T_m - T_{\infty})} \tag{27}$$

The applied force creates shear stress over the deformation zone. To describe this, an additional nondimensional parameter is defined that relates the loading level with respect to the material's shear strength. This parameter is $\tau^{\wedge}$, the ratio of shear stress due to friction to yield strength. This process parameter is "nondimensional applied stress $(\tau^{\wedge})$" as defined below:

$$\tau^{\wedge} = \frac{\mu.F_{ap}}{A_{DZ}.\tau_{yield}}. \tag{28}$$

A computer code calculates the values of q_f and q_w by using the applied force and sonotrode velocity and substitutes them into Eq. (23). The nondimensional problem is solved for 3 different nondimensional power inputs. The computer code was written with Visual Basic programming language following the flowchart shown in Figure 9. The material properties used are those for aluminum 6061-T6.

7. Results

Figure 10 shows the variation of nondimensional critical temperature for stick/slip change versus nondimensional applied stress for Al 6061-T6. This figure was obtained by using the variation shown in Figure 6 and the definitions of nondimensional temperature and nondimensional applied shear stress. As seen in this figure, as the nondimensional applied load increases, the nondimensional critical temperature for stick/slip shift decreases. Hence, the amount of energy required to transition from slip to stick decreases as the load is increased. Hence, at higher loads we expect a larger fraction of heat to be generated by plastic deformation than friction.

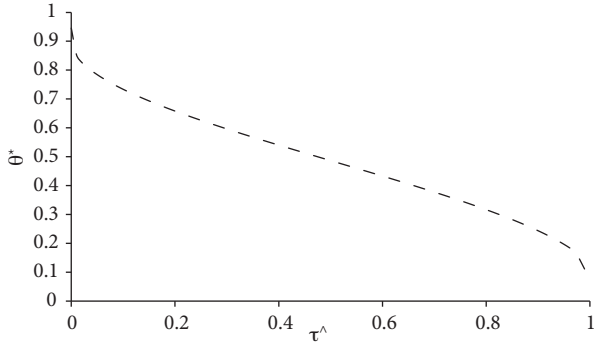

Figure 10. Variation of nondimensional critical temperature for stick/slip phase change as a function of nondimensional applied stress.

As seen in Eq. (27), the applied vibration amplitude directly affects the power input. On the other hand, according to Eqs. (17)–(23) and (26), the part thickness is effective in determining the elastic limits. This allows one to determine the regions where frictional heat generation and deformational heat generation dominate.

As seen from Eqs. (22) and (23), the main heat generation mechanisms are frictional heat generation and deformational heat generation. It is concluded from Eqs. (17) and (23) that for only frictional heat generation to be active, the applied vibration amplitude needs to be very small. By considering the force values at which most welding machines operate, the applied vibration amplitude needs to be smaller than 0.2 μm. However, this value strongly depends on foil thickness. For example, for aluminum foil with a thickness of 1 mm, the amplitude that causes only frictional heat generation should be less than or equal to 2 μm, which is lower than the operating range of most welding machines.

Figure 11 shows the variation of nondimensional temperature versus nondimensional time for different nondimensional power inputs. As seen from this figure, at the initial stages of the process the temperature starts to increase and eventually reaches a steady state. Furthermore, as the power input is increased, higher heating rates are expected, which translates into higher temperatures.

Figure 12 shows the variation of the nondimensional parameter, P_1, versus nondimensional temperature for different nondimensional power inputs. As the nondimensional temperature increases, the nondimensional heat generation rate (P_1) decreases since the material softens and shear deformation becomes easier. The same behavior is seen in the case of different nondimensional power inputs. As anticipated, as the nondimensional power input increases, the nondimensional heat generation rate increases as a result of increased interfacial frictional heat generation. Figure 12 also shows that the maximum nondimensional temperature value increases with increasing nondimensional power input.

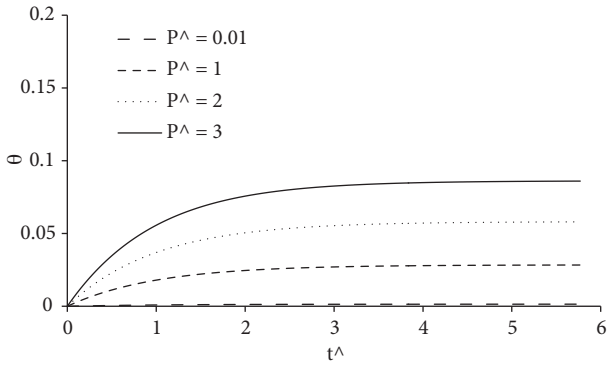

Figure 11. Variation of nondimensional temperature versus nondimensional time for different nondimensional power input (foil thickness: 100 μm, $\tau^{\wedge} = 0.10$).

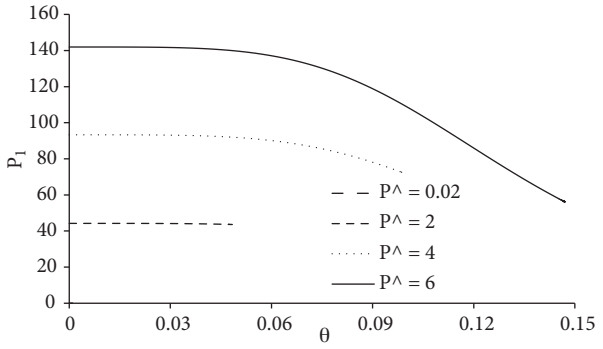

Figure 12. Variation of nondimensional parameter versus nondimensional temperature for different nondimensional power inputs (foil thickness: 100 μm, t = t_c, $\tau^{\wedge} = 0.2$).

By considering the operating range of most welding machines, the maximum nondimensional temperature for a thin foil is about 18% of its melting point.

Figures 13a and 13b show the variation of nondimensional temperature and nondimensional parameter P_1 during the welding process for very high applied load and applied amplitude. It is seen in this figure that the nondimensional temperature reaches a certain value and then remains constant. In Figure 13b, as the nondimensional parameter P_1 approaches unity, the system approaches a steady state.

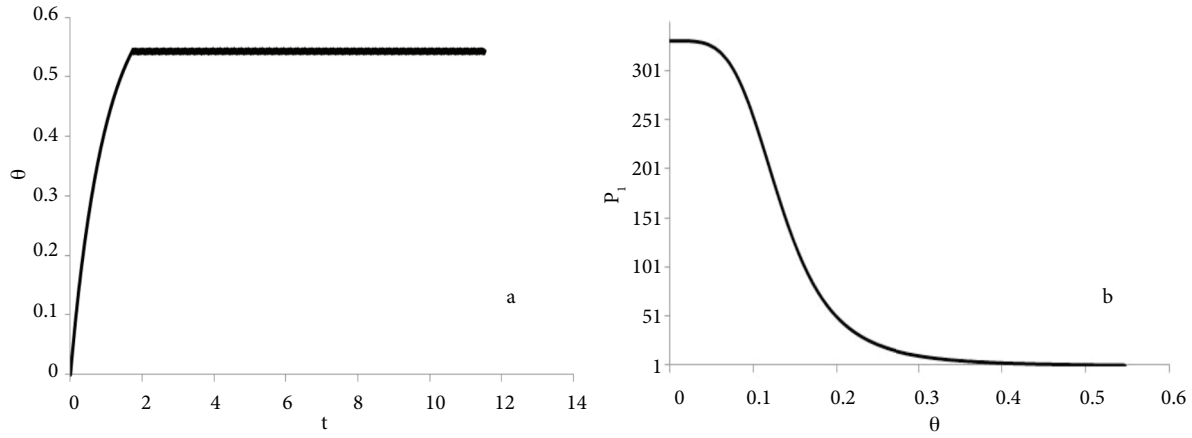

Figure 13. Variation of **a)** nondimensional parameter versus nondimensional temperature and **b)** nondimensional parameter P_1 versus nondimensional temperature (foil thickness: 100 μm, $P^{\wedge} = 13.2$, $\tau^{\wedge} = 0.4$).

Table 2 presents a comparison between predicted weld temperatures and reported experimental measurements [20]. As seen in this table, the predicted temperatures and experimental measurements are within 19% of each other on an average. This difference may be attributed to the following factors. The heat generation and heat transfer are 3-dimensional phenomena and these parameters should be obtained in 3 dimensions. However, UW is generally applied to the thin sheets and plates. Besides, welding needs a very short time to form. As expressed in Section 6, the selected parameters enable us to model this problem in 1 dimension. However, heat transfer in 3 dimensions might result in a difference between predicted and measure temperatures.

Table 2. Maximum welding temperatures for different test cases (assumed constant friction coefficient of 0.4).

Amplitude (μ)	Force (N)	Speed (mm/s)	Prediction (Current study, °C)	Experimental (Koelhoffer et al. 2011 [18], °C)	% Difference	% Contribution of friction	
						Initial	Final
16.9	1595	111	161.8	117.2	32	73	75
16.9	1018	99.2	117.3	130.1	10	63	65
13.9	1018	111	103.9	99.6	4	63	65
16.9	1307	87.2	138.5	121.7	13	69	71
13.9	1307	87.2	120.2	112.7	6	69	70
10.9	1018	123	90.2	76.7	16	63	63
13.9	1595	123	138.3	101.5	31	73	75
10.9	1307	99.2	102.5	83.0	21	68	70
10.9	1595	87.2	115.7	81.5	35	73	74
				Average	19	68	70

Another factor that might result in differences between measured and predicted values is the assumption of a constant friction coefficient. Experimental studies showed that the friction coefficient is not constant and can vary during the welding process. The frictional heat generation term and slip/stick state can change with the variation of the friction coefficient. In this study, the variation of the friction coefficient during welding was not determined and a constant friction coefficient was assumed.

Heavy plastic deformation and work hardening can result in inhomogeneous volumetric heat generation. This can also contribute to the difference between predicted and measured values.

Table 2 also shows the contribution of heat generation terms throughout the welding process. The contributions of different heat generation terms are not constant throughout the process. Since the deformation heat generation is temperature-dependent, its contribution to overall heat generation is not constant. The heat generation over the deformation zone has been obtained using Eqs. (4) and (7) and the contribution of frictional heat generation and deformational heat generation during the consolidation process has been evaluated for each weld by using a generated computer code. Average fictional contributions are on average 68% to 70% from weld initiation to cessation.

8. Summary and conclusions

In this study, the thermal modeling of continuous UW has been performed. Elastic limits for deformation, stick-slip phase change, and volumetric heat generation rates have been formulated. The heat transfer during the process has been formulated in a nondimensional form and solved using the fourth-order Runge–Kutta method. The predictions have been compared with reported experimental data. The results show that:

- The maximum allowable amplitude value for elastic deformation decreases with increasing temperature.
- During the UW process, 3 types of heat generation can occur. These are frictional heat generation, deformational heat generation, and heat generation due to elastic hysteresis. However, heat generation due to elastic hysteresis is very low in comparison with other heat generation terms and can be neglected.
- The nondimensional analysis reveals parameter P_1, which physically represents heat generated over heat dissipated. Initially, the heat generated is much higher than the heat convected, so P_1 is higher than unity. However, as the process continues, this parameter decreases, and for some cases it approaches unity at steady state.
- The slip phase changes to stick phase at a critical temperature depending on the applied interfacial shear stress as a result of oscillatory motion and applied force.
- As expected, the temperature seen at the interface increases with increasing nondimensional power input.
- The foil temperature depends on the nondimensional power input, nondimensional applied shear stress, and foil thickness. The foil surface temperature reaches up to 18% of the melting point of the material for most welding machines.
- Frictional heat generation and deformational heat generation exist at the same time in most cases.
- As a general conclusion, the temperature reaches it maximum value when $t^{\wedge}$ reaches 5 for applied nondimensional power inputs ($P^{\wedge}$) and nondimensional applied shear stress ($\tau^{\wedge}$) values that are encountered in most practical applications. This can serve as a guideline for the welding duration to avoid excessive plastic deformation and hardening of the material.
- The contribution of frictional heat generation and deformational heat generation during consolidation process has been evaluated for each weld. Average fictional contributions are on average 68% to 70% from weld initiation to cessation.

Acknowledgments

Author Ömer Sinan Şahin would like to thank Selçuk University (Turkey) and the Scientific and Technological Research Council of Turkey (TÜBİTAK), which financially supported him during his sabbatical visit to the Center for Composite Materials at the University of Delaware.

Nomenclature

F_{ap}	Applied force
δ_{app}	Applied vibration amplitude
$\delta_{\max}$	Amplitude limit for elastic working cond.
v_{avg}	Average vibration speed
T_∞	Ambient temperature
Bi	Biot number
t_c	Characteristic time
T^* and θ^*	Critical temperature for stick/slip phase change(real and nondimensional)
dA	Differential area
V	Volume
A_{DZ}	Deformation zone area
$\dot{q}_w$	Deformational heat generation rate (W/m^3)
dP	Differential power
ρ	Density
$P^\wedge$	Nondimensional power input
Ψ	Specific damping ratio
δ_{shear_p}	Deformation by plastic shear
L	Foil thickness
μ	Friction coefficient
$\dot{q}_{fr}$	Frictional heat generation rate (W/m^2)
F_{Fr}	Friction force
K(T)	Function determining the working cond.
k	Heat conduction coefficient
q_{total}	Total heat generation rate
h	Mean heat convention coefficient
T_m	Melting temperature
$\hat{t}$	Nondimensional time
P_1, P_2	Nondimensional parameters
P	Power
t	Real time
Δ	State variable
$\tau^\wedge$	Nondimensional applied stress
δ_{shear_e}	Deformation by elastic shear
γ	Shear angle
F_{shear}	Shear force
$\tau_{friction}$	Shear stress due to friction
c	Shear stiffness
G	Shear modulus
U	Strain energy
C_p	Specific heat
T	Temperature
θ	Nondimensional temperature
τ_y	Yield strength
W	Work
δ	Vibration amplitude
f	Vibration frequency
$\delta slip$	Slip distance
q_{eh}	Heat generation by elastic hysteresis (W/m^3)
τ_{ap}	Applied shear stress

References

[1] Kong CY, Soar RC, Dicens PM. Characterization of aluminum alloy 6061 for the ultrasonic consolidation process. Mat Sci Eng A-Struct 2003; 363: 99–106.

[2] Kong CY, Soar RC, Dicens PM. Ultrasonic consolidation for embedding SMA fibres within aluminum matrices. Compos Struct 2004; 66: 421–427.

[3] Kong CY, Soar RC, Dicens PM. Optimum process parameters for ultrasonic consolidation of 3003 aluminum. J Mater Process Tech 2004; 146: 181–187.

[4] Kong CY, Soar RC, Dicens PM. Model for weld strength in ultrasonically consolidated components. J Mech Eng Sci 2005; 1: 83–91.

[5] Langenecker B. Effects of ultrasound on deformation characteristics of metals. IEEE T Son Ultrason 1966; SU13: 1–8.

[6] Vairis A, Frost M. Modelling the linear friction welding of titanium blocks. Mat Sci Eng A-Struct 2000; 292: 8–17.

[7] Midling OT, Grong O. A process model for friction welding of Al-Mg-Si alloys and Al-Sic metal matrix composites-I. HAZ temperature and strain rate distribution. Acta Metall Mater 1994; 42: 1595–1609.

[8] Gould J, Feng Z. Heat flow model for friction stir welding of aluminum alloys. J Mater Process Manu 1998; 7: 185–194.

[9] Cheng X, Li X. Investigation of heat generation in ultrasonic metal welding using micro sensor arrays. J Micromech Microeng 2007; 17: 273–282.

[10] Benatar A, Cheng Z. Ultrasonic welding of themoplastics in far field. Polym Eng Sci 1989; 29: 1699–1704.

[11] Benatar A, Eswaran RV, Nayar S. Ultrasonic welding of themoplastics in near field. Polym Eng Sci 1989; 29: 1689–1698.

[12] Elangovan S, Semeer S, Prakasan K. Temperature and stress distribution in ultrasonic metal welding—An FEA-based study. J Mater Process Tech 2009; 209: 1143–1150.

[13] Sriramana MR, Gonser M, Fujii HT, Babu SS, Bloss M. Thermal transients during processing of materials by very high power ultrasonic additive manufacturing. J Mater Process Tech 2011; 211: 1650–1657.

[14] Siddiq A, Ghassemieh E. Thermomechanical analyses of ultrasonic welding process using thermal and acoustic softening effects. Mech Mater 2008; 40: 982–1000.

[15] De Vries E. Mechanics and mechanisms of ultrasonic metal welding. PhD, Ohio State University, Columbus, OH, USA, 2004.

[16] Du H, Klamecki BE. Force sensors embedded in surfaces for manufacturing and other tribiological process monitoring. J Manuf Sci E-T ASME 1999; 121: 739–748.

[17] Friswell MI, Inman DJ. Sensor validation for smart structures. J Intel Mat Syst Str 2000; 10: 973–982.

[18] Dieter GE. Mechanical Metallurgy. London, UK: McGraw-Hill; 1988.

[19] Maalekian M, Kozeschnik E, Brantner HP, Cerjak, H. Comparative analysis of heat generation in friction welding of steel bars. Acta Mater 2008; 56: 2843–2855.

[20] Koellhoffer S, Gillespie JW, Advani SG. Role of friction on the thermal development in ultrasonically consolidated aluminum foils and composites. J Mater Process Tech 2011; 211: 1864–1877.